Optimization of Electromagnetic Absorption in Laminated Composite Plates

Karel Matouš and George J. Dvorak

Abstract—**This paper analyzes an electromagnetic model of radar-absorbing layered structures for several stacking sequences of a woven glass/vinyl ester laminate, foam layers, and resistive sheets. It considers configurations that are either deposited on different backing materials or embedded in a laminated sandwich plate. Through-the-thickness layer dimensions and sheet resistances offering the best signal absorption over a specified frequency range are found for each configuration by minimizing an objective function with an enhanced genetic algorithm. The objective function includes selected values of minimum reflection coefficients and novel weight function distributions. In contrast to other optimization methods, this approach works with a population of initially selected values of the objective function and explores in parallel new areas in the search space, thus reducing the probability of being trapped in a local minimum. The procedure also yields the maximum reflection coefficient of −38.9 dB for a 0° incident wave passing through an optimized Jaumann absorber deposited on a metallic backing in the 7.5- to 18-GHz range, which corresponds to 5.2 times smaller reflected signal than a patented design. Two additional surface-mounted designs and three sandwich plate configurations are analyzed in a frequency band used by marine radars. In general, the surface-mounted designs have much lower reflection coefficients.**

Index Terms—**Electromagnetic energy, genetic algorithm, Jaumann absorber, reflection coefficient, resistive sheet, sandwich composite plate.**

I. INTRODUCTION

THE DESIGN of radar-absorbing materials is concerned with selection and spatial arrangement of dielectric and magnetic materials that provide a specified impedance profile to an incident wave [1], [2]. Theoretical foundations of the subject are well understood [3], [4] and provide a basis for specific applications. Several solution techniques leading to closed-form expressions, as well as relatively simple optimization schemes, have been proposed for maximizing absorption within a specified bandwidth [5]–[7]. Since the objective functions typically selected in optimization problems of this kind may have several local minima, it is preferable to use techniques that search for the absolute minimum, such as genetic algorithms [8]–[10].

The present work shows how the genetic algorithm approach can be enhanced and accelerated by incorporating novel weight functions and a replacement procedure based on the augmented simulated annealing. This is illustrated by comparisons with some available results. However, our primary objective is to show applications to the design of layered absorbers on ship structures, consisting of glass/epoxy laminates and a spacer foam interleaved with carbon sheets. Elements of the electromagnetic scattering theory needed to support such a design are incorporated into a genetic algorithm-based optimization procedure for minimization of an objective function within a prescribed frequency band. Several absorbing layer configurations, applied either at the surface or within a sandwich plate structure, are optimized for normal wave incidence.

The surface applications are represented by Jaumann-type absorbers, with an optimized distribution of both carbon sheet resistivities and foam spacer thicknesses deposited on a glass/epoxy laminate with a metallic and/or a free space backing. The classical Jaumann absorber configurations have been optimized with a genetic algorithm as shown, for example, by Chambers *et al.* [12], [13].

Using interior absorbing layers, separated by either two or three foam spacers of optimized thickness and bonded to exterior glass/epoxy laminates, is shown to offer a range of reflection coefficient values within the prescribed bandwidth, albeit not as attractive as those provided by the surface absorbers.

II. ELECTROMAGNETIC THEORY

Electromagnetic waves in a free space or a dielectric medium are governed by a set of Maxwell's equations, which relate field and flux variables among themselves and to sources

$$\nabla \times \boldsymbol{E} = -\frac{\partial \boldsymbol{B}}{\partial t}, \qquad \nabla \cdot \boldsymbol{B} = 0$$

$$\nabla \times \boldsymbol{H} = \boldsymbol{J} + \frac{\partial \boldsymbol{D}}{\partial t}, \qquad \nabla \cdot \boldsymbol{D} = \rho \tag{1}$$

where $\boldsymbol{E}[\text{V/m}]$ is electric field intensity, $\boldsymbol{D}[\text{C/m}^2]$ denotes electric displacement flux density, $\boldsymbol{H}[\text{A/m}]$ denotes magnetic field intensity, $\boldsymbol{B}[\text{Wb/m}^2]$ denotes magnetic induction, $\boldsymbol{J}[\text{A/m}^2]$ is electric current density, and $\rho[\text{C/m}^3]$ denotes electric charge density. The electromagnetic constitutive equations for an isotropic material are given by

$$\boldsymbol{D} = \epsilon_r \epsilon_0 \boldsymbol{E}, \quad \boldsymbol{B} = \mu_r \mu_0 \boldsymbol{H}, \quad \boldsymbol{J} = \sigma \boldsymbol{E} \tag{2}$$

where $\epsilon_0 = 8.854 \cdot 10^{-12}$ F/m, $\mu_0 = 0.4\pi \cdot 10^{-6}$ H/m are permittivity and permeability of the free space, $\epsilon_r = (\epsilon_r', \epsilon_r'')$, $\mu_r = (\mu_r', \mu_r'')$ are nondimensional complex relative material permittivity and permeability, and $\sigma[\text{S/m}]$ denotes the conductivity of the material. The wave equation for electric field in a conductive medium can be written in the form

$$\nabla^2 \boldsymbol{E} = -i\omega\mu(\sigma - i\omega\epsilon)\boldsymbol{E} \tag{3}$$
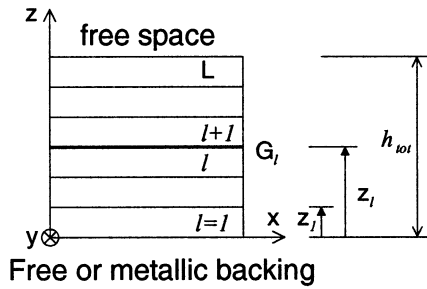
Fig. 1. Composite laminated plate.

where ω [rad/s] denotes circular frequency. All bold symbols represent vectors from $\mathbb{R}^3$

Evaluation of the reflection of an incident plane wave from an infinite flat multilayer structure involves application of boundary conditions, derived from Maxwell's equations, to the general solution for the electric and magnetic field in each layer [3]. Consider a composite laminated plate composed of L different dielectric layers, as shown in Fig. 1. It is assumed that impedance sheets of zero thickness are sandwiched between the layers. The complex form of the electric and magnetic fields associated with a normal plane wave in a given layer is

$$\hat{E} = \hat{E}^- \cdot e^{-ikz} + \hat{E}^+ \cdot e^{ikz}$$
$$|\hat{H}| = Y|\hat{E}| \tag{4}$$

where $\hat{E}^-$ and $\hat{E}^+$ represent the amplitudes of forward and backward propagating waves, and Y is the layer intrinsic admittance. The boundary conditions which must be satisfied at the interfaces are

$$G\hat{E}_{l+1} = G\hat{E}_l = \mathcal{J}$$
$$\hat{H}_{l+1} - \hat{H}_l = \mathcal{J} \tag{5}$$

where $G = 1/R^s$ [℧/□] is the sheet conductance, $R^s = 1/G[\Omega/□]$ is the sheet resistance, and $\mathcal{J}$ is current flowing in the sheet.

A stepping procedure is developed by substituting (5) into (4), which yields expressions for the coefficients $\hat{E}_{l+1}^+$, $\hat{E}_{l+1}^-$ in the terms of $\hat{E}_l^+$, $\hat{E}_l^-$. Only one case can be considered for the normal incidence, where the coefficients $\hat{E}_{l+1}^+$ and $\hat{E}_{l+1}^-$ are given by

$$\hat{E}_{l+1}^- = \frac{e^{ik_{l+1}z_l}}{2Y_{l+1}} \left[\hat{E}_l^-(Y_{l+1}+Y_l+G)e^{-ik_l z_l} \right.$$
$$\left. + \hat{E}_l^+(Y_{l+1}-Y_l+G)e^{ik_l z_l} \right]$$
$$\hat{E}_{l+1}^+ = \frac{e^{-ik_{l+1}z_l}}{2Y_{l+1}} \left[\hat{E}_l^-(Y_{l+1}-Y_l-G)e^{-ik_l z_l} \right.$$
$$\left. + \hat{E}_l^+(Y_{l+1}+Y_l-G)e^{ik_l z_l} \right]. \tag{6}$$

Arbitrary values of the coefficients of the fields $\hat{E}_{l=1}^+$, $\hat{E}_{l=1}^-$ are assigned in the first interior layer $l = 1$, then the program steps back from the first layer outward to calculate the value of each $\hat{E}_l^+$, $\hat{E}_l^-$, $\forall l \in <2, L+1>$. For a free space backing beyond the structure, no wave will be traveling back to the $L+1$ layer, hence $\hat{E}_1^+ = 0$, $\hat{E}_1^- = 1$ at $z = 0$, $l = 1$. If there is a metallic backing instead of a free space, the total electric field must vanish, and

according to (4), $\hat{E}_1^+ = -\hat{E}_1^-$, at $z = 0$, $l = 1$. The assignment $\hat{E}_1^- = 1$, $\hat{E}_1^+ = -1$ satisfies this particular condition, but creates an arbitrary amplitude that ultimately cancels out when the reflection coefficient is calculated. The stepping sequence is iterated until the $L+1$ layer is reached, which is the free space outside the structure. Thus, the reflection coefficient $\bar{R}$ of the structure is simply

$$\bar{R} = \frac{\hat{E}_{L+1}^+}{\hat{E}_{L+1}^-}, \quad R[\mathrm{dB}] = 20\log|\bar{R}|. \tag{7}$$

III. DESIGN OF TAILORED MATERIAL SYSTEMS FOR OPTIMAL EM PERFORMANCE

The objective of tailored material systems design is to minimize the radar signature of marine structures. Although selection of a suitable exterior shape can provide a dramatic signature reduction over a limited range of aspect angles, absorption of the incident electromagnetic energy is the main line of defense against detection. The electromagnetic properties of layered radar absorbing materials systems that provide a specific impedance profile to an incident wave depend on the layup sequence of dielectric and magnetic layers and their properties. The loss mechanism is typically provided by carbon, which converts the electromagnetic energy into heat. Energy absorption, however, does not necessarily require carbon. For marine radars operating in microwave frequency range of 8–12 GHz, the absorbed bandwidth can be increased by protective sandwich plates that contain several resistive sheets separated by a spacer foam. Selection of useful designs and evaluation of their optimized dimensions for maximum absorption in a specified frequency range is described as follows.

A. Definition of an Objective Function

The goal is to find an optimized form of a real-valued vector $\boldsymbol{X} = \{x_1 \ldots x_v\}$ of v design variables corresponding to the thicknesses of the layers h_l[m] and to the conductances $G = 1/R_l^s$ [℧/□] of the sheets. For example, for a four-layer sandwich containing two resistive sheets, the vector has the form

$$\boldsymbol{X} = \{h_1, h_2, h_3, h_4, G_1, G_2\}, \quad k = 1, \ldots, v = 6. \tag{8}$$

In the context of genetic algorithms, the vector $\boldsymbol{X}$ is often referred to as a *chromosome*, and the variables x_k as *genes*. Floating point representation of genes is used in the present implementation. For the general design requirements outlined at the beginning of this section, we select a normalized objective function $\mathfrak{f}(\boldsymbol{X}) \in <0, 1>$ as a sum of least squares of reflection coefficients R_{ij} in decibels (7) through the frequency spectrum $i \in <0, n_f>$. If applied to a formulation involving oblique incidence, the objective function would have to be optimized for angles $j \in <0, n_a>$ of the incident wave. In this case

$$\mathfrak{f}(\boldsymbol{X}) = \frac{1}{R_{\mathrm{nor}}} \sum_{i=1}^{n_f} \sum_{j=1}^{n_a} w_i w_j [R_{\min} - R_{ij}]^2 + \sum_{k=1}^{v} p_k \tag{9}$$

where $R_{\min}$ is a desired reflection coefficient of the sandwich plate, n_f is the number of analyzed frequencies i, and n_a is the number of analyzed angles j. The normalization parameter R_{nor}
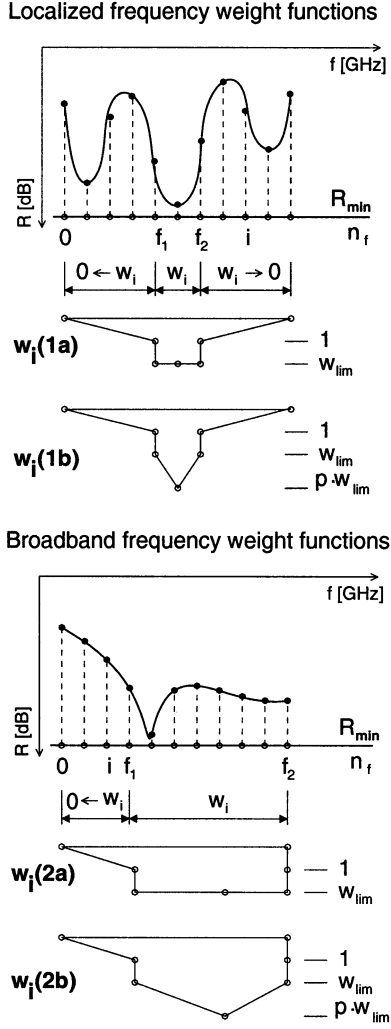
Fig. 2. Proposed frequency weight functions in selected frequency ranges.

Fig. 3. Proposed angle weight function in selected ranges of oblique incident waves.

denotes maximum reflectivity for $R_{ij} = 0$, $\sum_k^v p_k$ denotes sum of penalty functions, and w_i and w_j denote selected frequency and angle weight functions.

The specific weight functions w_i, w_j play a very important role in the optimization procedure, as they may substantially increase the efficiency of the optimization algorithm and provide the required shape of the objective function. In the absence of weight functions, the optimal solution is sought for in a large search space, while the problem at hand calls for such solutions in a smaller interval, defined by the radar bandwidth f_1, f_2. Two types of weight functions are developed in the present work, as shown in Figs. 2 and 3. Fig. 2 displays the localized types $w_i(1a)$ and $w_i(1b)$ that provide the shape of the objective function required within a selected interval of the radar bandwidth f_1, f_2. Efficient, low-reflectivity designs can be obtained in this manner, but their utility is limited to the selected interval. Fig. 2 also shows the broad-band weight functions $w_i(2a)$ and $w_i(2b)$, which cover a wider frequency spectrum but may yield higher reflectivity peaks than the localized functions. Fig. 3 illustrates proposed weight function selections w_j, for oblique incident waves, where the weight coefficients may be distributed to influence the optimal performance for specific angles of incidence.
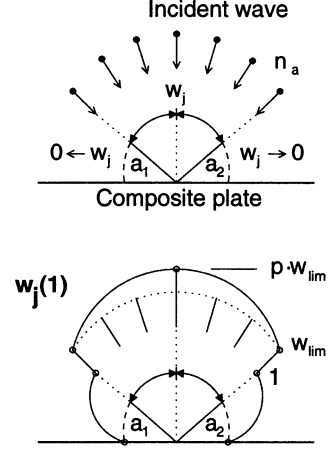
The last term $\sum_k^v p_k$ in (9) represents penalties to handle constraints, such as the minimum and maximum thickness of the layers and the minimum and maximum conductance of the sheets

$$h_{\min} \leq h_l \leq h_{\max}$$
$$G_{\min} \leq G_l \leq G_{\max}. \tag{10}$$

For example, in designs discussed in Section V, we selected $h_{\min} = 2$ mm for the foam layer and $h_{\min} = 5$ mm for the laminate, $h_{\max} = 30$ mm for both materials, $G_{\min} = 1/50$ ℧/□, $G_{\max} = 1/10\,000$ ℧/□. Values of the remaining parameters $R_{\min}$, n_a, n_f, f_1, f_2, v and selection of weight functions w_i, w_j are discussed in Section V.

The penalty function p_k assumes, in general, the form displayed in Fig. 4. Suppose that a variable $F_k = (h_1, \ldots, h_L, G_1, \ldots, G_L)$, $\forall k \in\, <1, v>$ should not exceed the allowable intervals (10)

$$F_{k,\min} \leq F_k \leq F_{k,\max}. \tag{11}$$

To formulate a penalty function p_k, we first introduce a parameter χ such that

$$\chi = |\bar{\chi}| \qquad \bar{\chi} = \frac{2}{F_{k,\min} - F_{k,\max}}(F_{k,\max} - F_k) + 1. \tag{12}$$

Since the constraints (11) are not violated in the closed interval $\chi < 1$, we let $p_k = 0$ there, as shown in Fig. 4. For $\chi > (1+\alpha)$, we set $p_k = \delta$, but for $\chi \in (1, 1+\alpha)$, we define

$$p_k = \gamma \left(\frac{\chi - 1}{\alpha} \right)^{\beta} \tag{13}$$

where α, β, γ, and δ are user-defined parameters. A large number is assigned to the parameter $\beta \to \infty$, whereas $\alpha \to 0$ and the parameter $\gamma \leq \delta$. For example, in the solutions discussed in Section V, for our case of a normalized objective function (9), $f(\boldsymbol{X}) \in\, <0, 1>$, we set $\beta = 5.0$, and $\gamma = \delta = 1.0$. For $\alpha = 0.05$, the design variable x_k can exceed minimum and maximum values by 5%, with the penalization p_k of the normalized objective function $f(\boldsymbol{X})$.
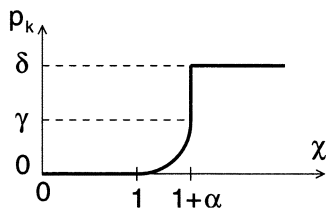
Fig. 4.   Proposed penalty function.

B. Optimization Techniques

Genetic algorithms work simultaneously with a population of individuals, exploring a number of new areas in the search space in parallel, thus reducing the probability of being trapped in a local minimum. This process is briefly described in Algorithm 1.

```
Algorithm 1: Principle of genetic algorithm
1  g = 0
2  generate and evaluate population P_g of size N
3  while (not termination-condition){
4    select m individuals to M_g from P_g
     (apply sampling mechanism)
5    alter M_g (apply genetic operators)
6    create and evaluate P_{g+1} from M_g
     (insert m new individuals into P_{g+1})
7    g = g + 1
8  }
```

For our optimization problem, the population P_g in Algorithm 1 becomes a family of possible configurations of a sandwich composite laminated plate. For example, in a four-layer plate with the chromosome defined by (8), we have a population of N members

$$
\left.
\begin{aligned}
&\mathfrak{f}_1(\boldsymbol{X}_1),\ \boldsymbol{X}_1 = \left\{ h_1^1, h_2^1, h_3^1, h_4^1, G_1^1, G_2^1 \right\} \\
&\qquad \vdots \qquad \vdots \qquad \vdots \\
&\mathfrak{f}_i(\boldsymbol{X}_i),\ \boldsymbol{X}_i = \left\{ h_1^i, h_2^i, h_3^i, h_4^i, G_1^i, G_2^i \right\} \\
&\qquad \vdots \qquad \vdots \qquad \vdots \\
&\mathfrak{f}_N(\boldsymbol{X}_N),\ \boldsymbol{X}_N = \left\{ h_1^N, h_2^N, h_3^N, h_4^N, G_1^N, G_2^N \right\}
\end{aligned}
\right\} \Rightarrow P_g
$$

(14)

where $\mathfrak{f}_i(\boldsymbol{X}_i)$ denotes value of the objective function or "fitness" of the ith chromosome. The first population P_0 can be created randomly, but an informed choice incorporated within the starting chromosome (SC) might decrease the number of GA iterations for an otherwise random population $(\boldsymbol{X}_1^{\text{SC}}, \boldsymbol{X}_2, \cdots \text{random} \cdots, \boldsymbol{X}_N) \in P_0$. A detailed description of the starting chromosome $\boldsymbol{X}_1^{\text{SC}}$ is given for solved examples in Section V.

The mating pool M_g represents a space for reproduction of offspring and consists of $m \geq 2$ chromosomes. The termination condition in Step 3 of Algorithm 1 is determined by a chosen number of GA iterations or by a population convergence criterion. The optimization examples in Section V were solved with population size $N = 600$, and with $m = 10$ chromosomes in the mating pool M_g in each algorithm cycle. The termination criterion was set at 6000 genetic algorithm iterations and a convergence criterion was not used.

1) Description of Main Steps of Algorithm 1:

a) Step 4: We already know from our earlier work [15], [16] that a proper selection strategy may significantly influence ultimate performance of the GA. The selection scheme should not be based on the exact fitness values $\mathfrak{f}_i(\boldsymbol{X})$. In such a case, the best individuals may appear in a large number of copies in a population, so that after a small number of GA cycles, all individuals start to look alike and the algorithm usually converges prematurely to a local minimum. Care must also be taken to avoid overcompression, which not only slows down the GA performance, but may result in the loss of the global minimum [17]. Therefore, a linear scaling (shifting) of the fitness was incorporated into our sampling procedure

$$
\mathfrak{s}_i(\boldsymbol{X}) = \frac{(N-1)\left(\mathfrak{f}_i(\boldsymbol{X}) - \mathfrak{f}_{\min}(\boldsymbol{X})\right)}{\mathfrak{f}_{\max}(\boldsymbol{X}) - \mathfrak{f}_{\min}(\boldsymbol{X})} + 1 \qquad (15)
$$

where $\mathfrak{f}_{\min}(\boldsymbol{X})$ and $\mathfrak{f}_{\max}(\boldsymbol{X})$ denote minimum and maximum fitness within a population, respectively. Thus, the fitness of chromosome $\mathfrak{f}_i(\boldsymbol{X}) \in\ <\mathfrak{f}_{\min}(\boldsymbol{X}), \mathfrak{f}_{\max}(\boldsymbol{X})>$ is linearly scaled to the interval $\mathfrak{s}_i(\boldsymbol{X}) \in\ <1, N>$.

In selecting the $m = 10$ individuals from a population P_g for mating and copying into the mating pool M_g, we implemented the sampling mechanism called *remainder stochastic sampling without replacement* (RSSwoR), commonly called *roulette wheel* [17]–[19]. There are N intervals on the roulette wheel. These intervals are not even as in a normal roulette wheel, but equal to the probability of selection of each individual. For a maximization problem, this probability $P_i(\boldsymbol{X})$ for each chromosome is defined by

$$
P_i(\boldsymbol{X}) = \frac{\mathfrak{e}_i(\boldsymbol{X})}{\sum_1^N \mathfrak{e}_i(\boldsymbol{X})}, \quad \mathfrak{e}_i(\boldsymbol{X}) = \frac{1}{\psi + \mathfrak{s}_i(\boldsymbol{X})}, \quad \mathfrak{s}_i(\boldsymbol{X}) \geq 0
$$

(16)

whereas $\mathfrak{e}_i(\boldsymbol{X}) = \mathfrak{s}_i(\boldsymbol{X})$ when solving a minimization problem. The parameter ψ is a small positive number that eliminates the possibility of division by zero. In the sampling procedure, the fitness $\mathfrak{s}_j(\boldsymbol{X})$ of the selected individual $j \in\ <1, m>$ is set equal to zero after each spin (selection) j to prevent multiple selections of the same chromosome in the next spins $j = j + 1$, $\forall j \leq m$.

b) Step 5: With reference to (8), (10), and (11), we denote a parent chromosome by $\boldsymbol{X} = \{x_1, \ldots, x_v\}$ and an offspring by $\boldsymbol{X}' = \{x_1', \ldots, x_v'\}$. The variables x_k, $k \in\ <1, v>$ represent thicknesses of the layers and conductances of the resistive sheets. Two types of genetic operators are applied to all $m = 10$ individuals in the current mating pool M_g: a mutation operator that generates an offspring by changing a single variable in a parent chromosome, and a crossover operator that creates an offspring by combining variables of two parent chromosomes.

The type of operator (mutation and/or crossover) is selected with a certain probability, depending on the population and mating pool size. Let P_{mut} and P_{cro} be chosen probabilities of selection of the mutation and crossover operators in the genetic algorithm cycle, respectively. A crossover operator is selected if a random number $r < P_{\text{cro}}$, $r \in\ <0, 1>$. In the opposite case $r \geq P_{\text{cro}}$, a mutation operator is applied. The probability of mutation was set at $P_{\text{mut}} = 0.7 \Rightarrow P_{\text{cro}} = 0.3$

for all optimization problems. The various types of mutation and/or crossover operators for floating-point representation, such as *uniform mutation, boundary mutation, nonuniform mutation, simple crossover,* and *simple arithmetic crossover,* are selected uniformly through genetic cycles. Details regarding construction of these genetic operators can be found in [18] and [20].

c) Step 6: The replacement procedure in our algorithm, where individuals in the mating pool replace the unfit chromosomes in a population, is subject to the Metropolis criterion from the *augmented simulated annealing method* (ASA) [21]. This criterion allows, with a certain probability, a worse offspring to replace its better parent, and the probability is reduced by a "temperature" parameter T as the procedure converges to the global minimum. An inverse roulette wheel routine is used, with the inverted fitness of individuals, which provides the m weakest individuals in the population P_g with a higher probability to die out. Replacement of the m individuals in the population with those from the mating pool $M_g \to P_{g+1}$ is realized if the fitness of an offspring in the mating pool is higher than that of those marked for dying out, $\mathfrak{s}_i(X') < \mathfrak{s}_i(X)$, or if the probability of accepting is $r \le P_{\text{ex}}$, $r \in\, <0,1>$

$$P_{\text{ex}} = \exp\left(-\frac{[\mathfrak{s}_i(X') - \mathfrak{s}_i(X)]}{T}\right) \quad (17)$$

where $\mathfrak{s}_i(X)$ is defined in (15). The temperature T is bracketed by $T_{\min} \le T \le T_{\max}$, where $T_{\min}$ is the value at the termination of the process, and $T_{\max}$ should be chosen such that the ratio of accepted solutions to all solutions is approximately equal to $0.5 \approx 50\%$. Temperature decrease is controlled by $T_{g+1} = T_{\text{cool}}T_g$, where $T_g = T_0 = T_{\max}$, $g = 0$. This process is called the *cooling schedule*. All parameters $T_{\min}$, T_{cool}, and $T_{\max}$ must be suitably chosen; therefore, the annealing schedule requires some experimentation depending on the optimization problem, number of members in the population N, and maximum number of iterations $g_{\max}$. For all optimization examples in Section V, with a normalized objective function and first average value of fitness in a population approximately equal to 0.8, we set this cooling schedule as $T_{\max} = 0.05$, $T_{\text{cool}} = 0.999$, and $T_{\min} = 0.00001$.

2) Convergence of the Genetic Algorithm: Convergence depends strongly on the information stored in genes of chromosomes in the population. If the population does not contain the information necessary to reach the expected results, mutations are only one way to create them. The genetic algorithm then needs a large number of generation cycles. The number of iterations can be reduced by several useful techniques. If convergence of the algorithm is very slow, one can restart the optimization process to create any missing information, which is represented by genes composing the chromosomes. The several best members of a population are copied to the next population, and the remaining individuals are created randomly to input new information. The optimization process then continues with the same optimization parameters, or can be started again from the beginning. This process is called reoptimization, or reannealing for ASA [21].
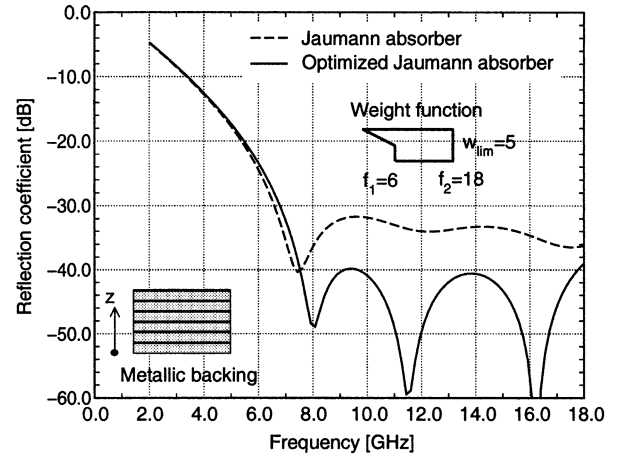

Fig. 5. Performance comparison of the patented and optimized Jaumann absorbers in the frequency range of 8–18 GHz.

TABLE I
THICKNESS h_l [mm] OF FOAM AND RESISTANCE $R_l^s = 1/G_l[\Omega/\square]$ OF SHEETS IN JAUMANN ABSORBER

Solution	before optimization: $R_{max} = -32$ dB		after optimization: $R_{max} = -39$ dB	
layer	thickness h_l	resistance $R_l^s = 1/G_l$	thickness h_l	resistance $R_l^s = 1/G_l$
1	3.56	236	3.56	236
2	3.56	471	3.52	481
3	3.56	943	3.56	943
4	3.56	1508	3.26	1543
5	3.56	2513	3.79	2567
6	3.56	9425	4.18	9465

TABLE II
ELECTROMAGNETIC MATERIAL PROPERTIES

	Permittivity, ϵ_r		Permeability, μ_r	
Material	ϵ_r'	ϵ_r''	μ_r'	μ_r''
Woven E-glass/vinyl ester	3.07	0.056	1.0	0.0
Core foam, spacer	1.03	0.0001	1.0	0.0

IV. JAUMANN ABSORBER TEST CASE

To verify the efficiency of our approach, we first optimized the six-layer Jaumann absorber with the metallic backing [11]. The patented configuration, shown schematically in the inset of Fig. 5, consists of six dielectric foam spacer layers of thickness 3.56 mm and six resistive sheets of different resistivities. The second and third columns of Table I list the foam layer thicknesses and resistivities of the carbon sheets. Electromagnetic properties of the foam layer appear in Table II. Only normal incidence was considered and the first population P_0 was assembled of $N = 600$ randomly created chromosomes. However, one chromosome X_1^{SC} was generated using the patented parameters, which are listed in Table I. The broad-band frequency weight function $w_i(2a)$ was used together with the following parameters in the objective function (9).

- Number of design variables $v = 12$, $X = \{h_1, \ldots, h_6, G_1, \ldots, G_6\}$.
- $f \in (2, 18)$ GHz, number of frequencies $n_f = 100$.
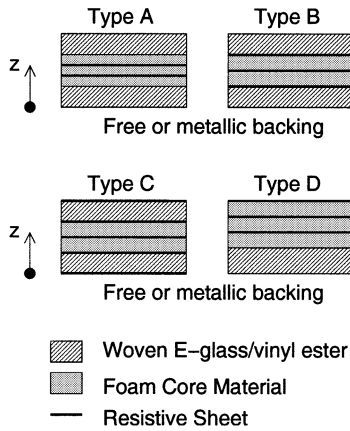- $\angle a = 0.0$, number of angles $n_a = 1$.
- $R_{\min} = -50.0$ dB.

Fig. 6. Examples of analyzed embedded and surface mounted absorber configurations.

TABLE III
PARAMETERS USED IN OPTIMIZATION OF TYPE A–D ABSORBERS

Absorber Type	w_i	w_{lim}	p	f_1 GHz	f_2 GHz	R_{min} dB	Lines in Figs. 7-9
$A_1 - C_1$ - free backing	$w_i(1a)$	5.0	-	8.0	12.0	−25.0	dashed
$A_2 - C_2$ - free backing	$w_i(1b)$	3.0	2.0	8.0	12.0	−25.0	dotted
$A_3 - C_3$ - free backing	$w_i(1b)$	3.0	1.5	7.0	13.0	−25.0	solid
D_1 - free backing	$w_i(1a)$	5.0	-	7.0	15.0	−45.0	solid
D_2 - free backing	$w_i(1a)$	5.0	-	6.0	18.0	−45.0	dashed
D_2 - metallic backing	$w_i(2a)$	5.0	-	6.0	18.0	−45.0	dotted

- Angle weight function $w_j(1) = 1$.
- Frequency weight function $w_i(2a)$, $f_1 = 6.0$ GHz, $f_2 = 18.0$ GHz, $w_{\lim} = 5.0$.

The optimization procedure was repeated several times with similar outputs. Slightly better results were obtained with a reoptimization that included one of the fittest chromosomes. The best result obtained for the Jaumann absorber is shown by the solid line in Fig. 5, which indicates that the maximum reflection coefficient in the 7.5- to 18-GHz range has been reduced from −31.7 dB of the patented design to −38.9 dB; the reflected signal is 5.2 times smaller than the patented design. Optimized values of the design variables are listed in the fourth and fifth columns of Table I. The Jaumann-type absorbers have also been optimized with other genetic algorithms; for example, by Chambers *et al.* [12], [13] who obtained $R_{\max} = -20$ dB reflectivity bandwidths for three- and/or four-layer absorbers.

V. EXAMPLES

The described optimization procedure was applied to several numerical examples related to applications in laminated sandwich plates exposed to marine radars, which usually operate in the frequency range of 8–12 GHz. Only the normal incident waves are considered in the computations. In a typical configuration, a foam layer is sandwiched between two layers made of a woven E-glass/vinyl ester laminate. Interleaved resistive carbon sheets are added to create an absorber. Fig. 6 shows the configurations of three embedded $(A$–$C)$ and one surface (D) absorber, optimized herein under different assumptions and constraints. Although the laminate and core thicknesses were kept within a
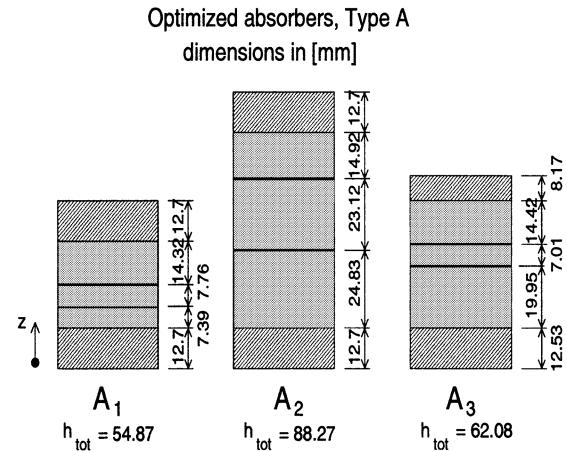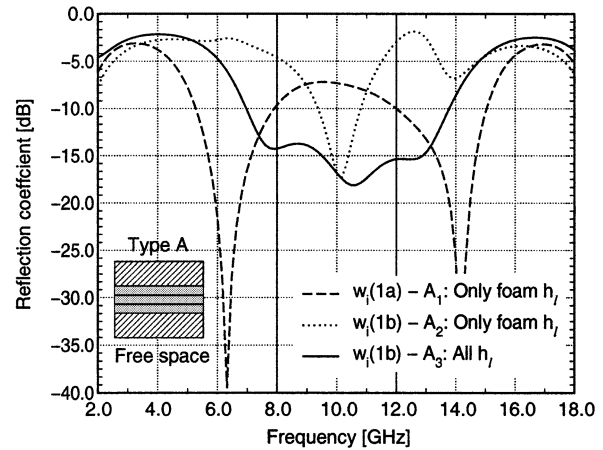

Fig. 7. Reflection coefficients of embedded Type A layups, with sheet resistivities and foam and/or laminate thicknesses optimized using different weigh functions in the 8- to 12-GHz range.

reasonable range, no attempt was made to include mechanical performance criteria, such as strength or stiffness, in the optimization procedures. Electromagnetic material parameters are listed in Table II. Due to lack of needed material property data, all electromagnetic properties for a woven E-glass/vinyl ester were taken from Mumby *et al.* [22], as equal to those for an epoxy resin and e-PTFE+E-glass fibers. Similar material data are presented by Moore *et al.* [23] for Kevlar or Astroquartz fibers and epoxy resin. The material parameters are assumed to remain constant through the frequency spectrum of the incident wave.

The sets of weight function parameters and $R_{\min}$ values needed in (9) were selected on the basis of parametric studies and applied to each of the Type A, B, and C absorbers; their values appear in Table III, together with those selected for the Type D absorbers. The initial populations P_0 were created randomly for all sandwich plates. Type A and B absorbers employ, respectively, two and three resistive sheets completely embedded inside the sandwich plate. Only one of the three resistive sheets is inside the core in Type B, while the other two reside at the foam-laminate interfaces; hence, this layup sequence should be as easy to fabricate as that of Type A. Type C adds two resistive sheets at both outer surfaces of the laminates to the Type B configuration, for a total of
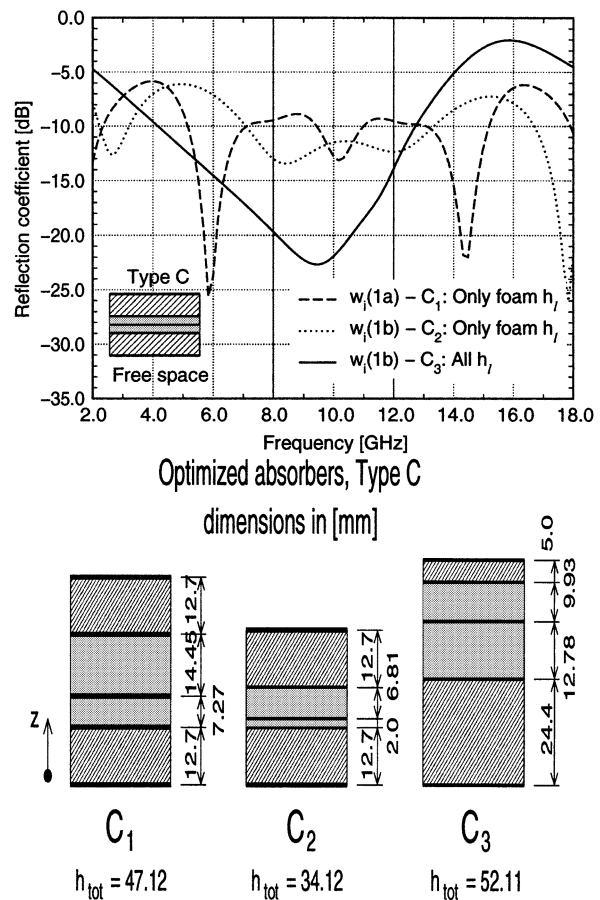
Fig. 8. Reflection coefficients of embedded Type B layups, with sheet resistivities and foam and/or laminate thicknesses optimized using different weigh functions in the 8- to 12-GHz range.
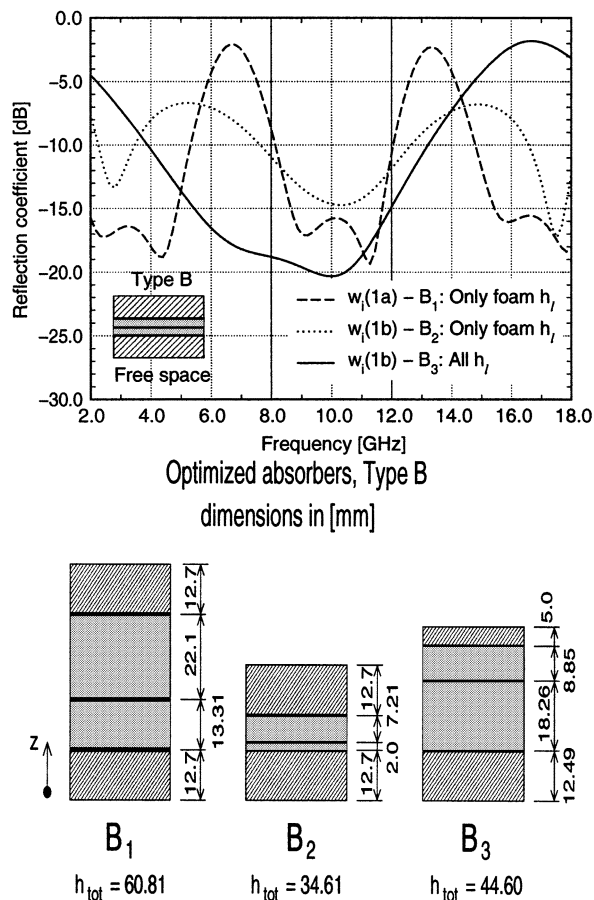

Fig. 9. Reflection coefficients of embedded Type C layups, with sheet resistivities and foam and/or laminate thicknesses optimized using different weigh functions in the 8- to 12-GHz range.

five resistive layers. As indicated by (10), constraints were prescribed on the maximum and/or minimum thickness of the individual foam and laminate layers, and on the resistivities of the carbon sheets. Moreover, the laminate layers thickness was prescribed as equal to 12.7 mm, (0.5 in), except in the Types A_3, B_3, and C_3, where the laminate thickness was optimized together with the foam layer thicknesses and sheet resistivities. However, the total thickness h_{tot} of the sandwich plates was left unconstrained. This produced many different total thicknesses with optimized absorption properties. Structural strength and stiffness requirements that may impose other thickness constraints could be included in the present procedure.

Results obtained for the embedded configurations A–C with free backing are shown in Figs. 7–9 and Tables IV–VI. In each figure, the dashed lines represent reflection coefficients computed with the $w_i(1a)$ weight function, fixed laminate layer thicknesses of 12.7 mm (0.5 in), and optimized foam thicknesses and sheet resistivities; the resulting configurations are denoted as A_1, B_1, and C_1. The dotted lines show reflection coefficients computed for the same free and fixed variables with the localized $w_i(1b)$ weight function, resulting in configurations denoted as A_2, B_2, and C_2. Finally, the solid lines refer to results obtained from solutions optimizing both foam layer and laminate thicknesses as well as sheet resistivities with the less localized $w_i(1b)$ frequency weight function. These

TABLE IV
THICKNESSES h_l [mm] OF LAYERS AND RESISTANCES R_i^s [$\Omega/\square$] OF SHEETS FOR TYPE A ABSORBERS

Solution	Laminate h_1	Foam h_2	Foam h_3	Foam h_4	Laminate h_5	R_1^s	R_2^s
$w_i(1a)$-A_1: foam h_l	12.7	7.39	7.76	14.32	12.7	423.79	755.57
$w_i(1b)$-A_2: foam h_l	12.7	24.83	23.12	14.92	12.7	51.8	168.17
$w_i(1b)$-A_3: each h_l	12.53	19.95	7.01	14.42	8.17	50.19	332.30

TABLE V
THICKNESSES h_l [mm] OF LAYERS AND RESISTANCES R_i^s [$\Omega/\square$] OF SHEETS FOR TYPE B ABSORBERS

Solution	Laminate h_1	Foam h_2	Foam h_3	Laminate h_4	R_1^s	R_2^s	R_3^s
$w_i(1a)$-B_1: foam h_l	12.7	13.31	22.1	12.7	50	50	175.01
$w_i(1b)$-B_2: foam h_l	12.7	2.0	7.21	12.7	77.16	50	185.0
$w_i(1b)$-B_3: each h_l	12.49	18.26	8.85	5.0	10000	50	158.07

TABLE VI
THICKNESSES h_l [mm] OF LAYERS AND RESISTANCES R_i^s [$\Omega/\square$] OF SHEETS FOR TYPE C ABSORBERS

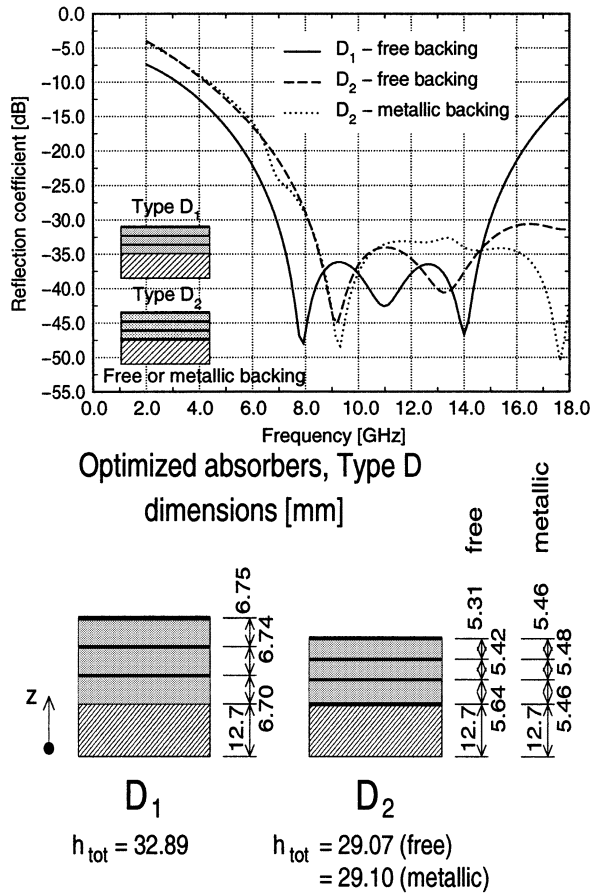| Solution	Lam. h_1	Foam h_2	Foam h_3	Lam. h_4	R_1^s	R_2^s	R_3^s	R_4^s	R_5^s
$w_i(1a)$-C_1: foam h_l	12.7	7.27	14.45	12.7	265.5	10000	477.5	784.89	10000
$w_i(1b)$-C_2: foam h_l	12.7	2.0	6.81	12.7	73.5	50	50	221.97	10000
$w_i(1b)$-C_3: each h_l	24.4	12.78	9.39	5.0	758.0	63.68	50	145.31	10000

Fig. 10. Reflection coefficients of embedded Type D layups, with sheet resistivities and foam and/or laminate thicknesses optimized using different weigh functions in the 8- to 18-GHz range.

TABLE VII
THICKNESSES h_l [mm] OF LAYERS AND RESISTANCES $R_i^s [\Omega/\Box]$ OF SHEETS FOR TYPE D ABSORBERS

Solution	$\frac{\text{Lam.}}{h_1}$	$\frac{\text{Foam}}{h_2}$	$\frac{\text{Foam}}{h_3}$	$\frac{\text{Foam}}{h_4}$	R_1^s	R_2^s	R_3^s	R_4^s
Type D_1-free	12.70	6.697	6.744	6.748	-	438.175	791.146	2549.775
Type D_2-free	12.70	5.637	5.417	5.314	50.0	277.335	755.521	2992.971
Type D_2-metallic	12.70	5.463	5.480	5.463	50.0	277.335	755.521	3006.05
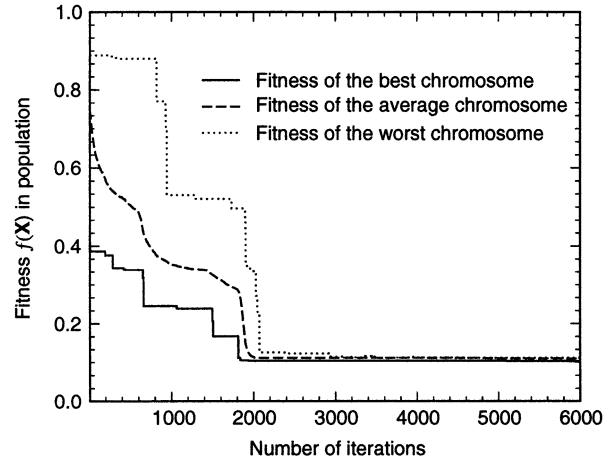
Fig. 11. Convergence of the genetic algorithm for Type D_2 with free space backing.

are denoted as A_3, B_3, and C_3. As expected, selecting the weight function $w_i(1a)$ provides more uniform reduction of the reflection coefficient within the frequency range f_1 and f_2 (Fig. 2). On the other hand, the $w_i(1b)$ weight function yields low-reflection coefficient values close to the middle of the $f_1 - f_2$ bandwidth. Constraining the laminate layers thickness values, as may often be dictated by structural requirements, tends to impair absorption capacity. Removing this constraint results in lower reflection coefficients, but also in thinner outer laminated layers; these may be accommodated in certain structural parts. Comparison of the results shows that the Type A_1 and A_2 absorbers have the highest reflection coefficient values in the selected frequency range. Adding the third resistive sheet and using the Type B_1 or B_2 configurations improves the performance somewhat. However, the surface resistive sheets in Type C_1 and C_2 absorbers yield negligible performance improvement. The most significant reduction in the reflection coefficients is obtained by including the laminate thicknesses among the optimized variables. This provides $R_{max} < -15$ dB in both Type B_3 and C_3 and $R_{max} < -13.7$ dB in Type A_3.

Inspired by the superior performance of the Jaumann absorber, we analyzed several surface absorbers of Type D, with either free or metallic backing. Fig. 10 and Table VII present the results, with three resistive sheets and free backing in Type D_1, and four sheets and either free or metallic backing in Type D_2. The presented surface absorber configurations provide

much lower reflection coefficients than the above Types A–C, with $R_{max} = -30.6$ dB for Type D_2 within 8- to 18-GHz bandwidth, and $R_{max} = -36.2$ dB for Type D_1 in the 7.5- to 14.5-GHz interval. Good absorption was obtained for both free and metallic backing of Type D_2, with very similar optimized design variables. Such a result suggests good efficiency of electromagnetic absorption for this structure regardless of backing. Although employing only three foam layers and three or four resistive sheets, the Type D absorbers offer performance comparable to that of the optimized Jaumann absorber with six foam layers and resistive sheets.

Fig. 11 illustrates the rate of convergence of the optimization procedure that was applied to the Type D_2 absorber. Fitness of the best chromosome in a randomly created population is $f(X) = 0.408$ and it drops to $f(X) = 0.103$ at completion of the optimization process. This represents 25.2% improvement over random design of the best individual and 14.5% improvement over the average fitness of the chromosomes in the population, where $f(X) = 0.760 \rightarrow f(X) = 0.110$.

VI. CONCLUSION

A modified genetic algorithm, enhanced by the ASA replacement procedure and the novel weight functions, is used here in design of optimized radar absorbing sandwich structures for marine applications. Efficiency of the procedure has been tested by optimizing the patented Jaumann absorber consisting of six dielectric foam layers of constant thickness and variable resistivities of six resistive carbon sheets. When both the sheet resistivities and foam layer thicknesses were included among the optimized variables, our procedure yielded $R_{max} = -38.9$ dB; the reflected signal is 5.2 times smaller than the patented design in the 7.5- to 18-GHz frequency range.

Similar surface absorbers, Type D, consisting of only three foam layers and three and/or four resistive sheets, were also found to be very effective. Type D absorbers yielded reflection coefficients $R_{max} = -30.6$ dB in the 8- to 18-GHz frequency range for Type D_2 and $R_{max} = -36.2$ dB in the 7.4- to 14.5-GHz bandwidth for Type D_1.

For applications that require placing of the absorbing layers within a sandwich plate with glass/epoxy laminate faces, the present results suggest three design alternatives involving different numbers of absorbing layers with optimized resistivity values and spacer thicknesses (Figs. 7–9). However, the high permittivity and thickness of the laminate surface layer impairs the absorbing capacity of the embedded designs. Although the design optimization was constrained within the narrower 8- to 12-GHz bandwidth preferred by some marine radars, we found the lowest value of the reflection coefficient of only $R_{max} = -15.0$ dB. Of course, higher values would be obtained in a broader frequency range. In contrast, $R_{max} = -30.6$ and -36.2 dB was reached in the same narrower bandwidth with the Type D designs (Fig. 10).

ACKNOWLEDGMENT

REFERENCES

[1] T. C. P. Wong, B. Chambers, A. P. Anderson, and P. V. Wright, "Fabrication and evaluation of conducting polymer composites as radar absorbers," in *8th Int. Conf. Antennas and Propagation ICAP'93*, vol. 2, 1993, pp. 934–937.

[2] R. S. Grannemann and M. I. Jones, "Electromagnetic scattering from a dielectric-coated sphere with an embedded impedance film," *IEEE Trans. Antennas Propagat.*, vol. 47, pp. 1340–1342, Aug. 1999.

[3] E. F. Knott, J. F. Shaeffer, and M. T. Tuley, *Radar Cross Section*. Norwood, MA: Artech House, 1993.

[4] J. A. Stratton, *Electromagnetic Theory*. New York: McGraw-Hill, 1941.

[5] H. Lidell, *Computer-Aided Techniques for the Design of Multilayer Filters*. Bristol, U.K.: Adam Hilger, 1981.

[6] C. F. Du Toit and J. H. Cloete, "Advances in design of Jaumann absorbers," in *Proc. IEEE-APS URSI Meet.*, Dallas, TX, 1990, pp. 248–252.

[7] J. Pesque, D. Bouche, and R. Mittra, "Optimization of multilayer antireflection coatings using an optimal control method," *IEEE Trans. Microwave Theory Tech.*, vol. 40, pp. 1789–1796, Sept. 1992.

[8] D. S. Weile, E. Michielssen, and D. E. Goldberg, "Genetic algorithm design of Pareto optimal broadband microwave absorbers," *IEEE Trans. Electromagn. Compat.*, vol. 38, pp. 518–525, Aug. 1996.

[9] E. Michielssen, J.-M. Sajer, S. Ranjithan, and R. Mittra, "Design of lightweight, broad-band microwave absorbers using genetic algorithms," *IEEE Trans. Microwave Theory Tech.*, vol. 41, pp. 1024–1031, June/July 1993.

[10] T. A. Cusick, S. Iezekiel, and R. E. Miles, "All-optical microwave filter design employing a genetic algorithm," *IEEE Photon. Technol. Lett.*, vol. 10, pp. 1156–1158, Aug. 1998.

[11] T. M. Connolly and E. J. Luoma, "Microwave Absorber," U.S. Patent 4 038 660, July 1977.

[12] B. Chambers and A. Tennant, "Optimized design of Jaumann radar absorbing materials using a genetic algorithm," *Inst. Elect. Eng. Proc.—Radar Sonar Navigat.*, vol. 143, pp. 23–30, Jan. 1996.

[13] ——, "Design of wideband Jaumann radar absorbers with optimum oblique incidence performance," *Electron. Lett.*, vol. 30, no. 18, pp. 1530–1532, 1994.

[14] Z. Michalewicz, *Genetic Algorithms + Data Structures = Evolution programs*. New York: Springer-Verlag, 1992.

[15] K. Matouš, "Analysis and optimization of composite materials and structures," CTU Reports, Prague, vol. 4, 2000.

[16] K. Matouš, M. Lepš, J. Zeman, and M. Šejnoha, "Applying genetic algorithms to selected topics commonly encountered in engineering practice," *Comput. Meth. Appl. Mech. Eng.*, vol. 190, no. 13–14, pp. 1629–1650, 2000.

[17] D. E. Goldberg, *Genetic Algorithms in Search, Optimization and Machine Learning*. Harlow, U.K.: Addison-Wesley, 1989.

[18] Z. Michalewicz, T. D. Logan, and S. Swaminathan, "Evolutionary operators for continuous convex parameter spaces," in *Proc. 3rd Annu. Conf. Evolutionary Programming*, A. V. Sebald and L. J. Fogel, Eds., 1994.

[19] J. E. Baker, "Reducing bias and inefficiency in the selection algorithm," in *Proc. 2nd Int. Conf. Genetic Algorithms*, J. J. Grefenstette, Ed., 1987, pp. 13–21.

[20] C. R. Houck, J. A. Joines, and M. G. Kay, *A Genetic Algorithm for Function Optimization: A Matlab Implementation*. Raleigh: North Carolina State Univ., 1995.

[21] V. Kvasnička, "Augmented simulated annealing adaption of feedforward neural networks," *Neural Network World*, vol. 3, pp. 67–80, 1994.

[22] S. J. Mumby, G. E. Johnson, and E. W. Anderson, "Dielectric properties of some PTFE-reinforced thermosetting resin composites," in *Proc. 19th Electrical Electronics Insulation Conf.*, Chicago, IL, 1989, pp. 263–267.

[23] R. L. Moore and A. MacDonald, "Permittivity of fiber polymer composites environmental effects: comparison of measurement and theory," in *Antennas and Propagation Soc. Int. Symp.*, vol. 3, 1990, pp. 1204–1207.

Karel Matouš is a postdoctoral Research Associate at Rensselaer Polytechnic Institute, Troy, NY. His research is primarily focused on multiscale numerical modeling of heterogeneous inelastic solids, high performance parallel computing and optimization techniques based on genetic algorithms and their applications.

Dr. Matouš is a Member of ASME, ASCE, and ASC.

George J. Dvorak is the William Howard Hart Professor of Mechanics at Rensselaer Polytechnic Institute, Troy, NY. His research is concerned with modeling of many aspects of mechanical behavior of composite materials and structures.

Dr. Dvorak is a Fellow of AAM, ASME, and SES, and a member of the National Academy of Engineering.